# Temperature dependent electronic transport in concentrated solid solutions of the 3*d*-transition metals Ni, Fe, Co and Cr from first principles

G. D. Samolyuk,[1,*] S. Mu,[1] A. F. May,[1] B. C. Sales,[1] S. Wimmer,[2] S. Mankovsky,[2] H. Ebert,[2] and G. M. Stocks[1]

[1]*Materials Science and Technology Division, Oak Ridge National Laboratory, Oak Ridge, Tennessee 37831, USA*
[2]*Department of Chemistry, Ludwig-Maximilian-Universitaet, D-81377 Muenchen, Germany*

An approach previously developed for the calculation of transport coefficients via the Mott relations is applied to the calculation of finite temperature transport properties of disordered alloys—electrical resistivity and the electronic part of thermal conductivity. The coherent-potential approximation is used to treat chemical disorder as well as other sources of electron scattering, i.e., temperature induced magnetic moment fluctuations and lattice vibrations via the alloy analogy model. This approach, which treats all forms of disorder on an equal first-principles footing, is applied to the calculation of transport properties of a series of fcc concentrated solid solutions of the 3*d*-transition metals Ni, Fe, Co, and Cr. For the nonmagnetic alloys $Ni_{0.8}Cr_{0.2}$ and $Ni_{0.33}Co_{0.33}Cr_{0.3}$, the combined effects of chemical disorder and electron-lattice vibrations scattering result in a monotonic increase in the resistivity as a function of temperature from an already large, $T = 0$, residual resistivity. For magnetic $Ni_{0.5}Co_{0.5}$, $Ni_{0.5}Fe_{0.5}$, and $Ni_{0.33}Fe_{0.33}Co_{0.33}$, the residual resistivity of which is small, additional electron scattering from temperature induced magnetic moment fluctuations results in a further rapid increase of the resistivity as a function of temperature. The electronic part of the thermal conductivity in nonmagnetic $Ni_{0.8}Cr_{0.2}$ and $Ni_{0.33}Co_{0.33}Cr_{0.33}$ monotonically increases with temperature. This behavior is a result of the competition between a reduction in the conductivity due to electron-lattice vibrations scattering and temperature induced increase in the number of carriers. In the magnetic alloys, electron scattering from magnetic fluctuations leads to an initial rapid decrease in thermal conductivity until this is overcome by an increasing number of carriers at temperatures slightly below the Curie temperature. Similar to the resistivity above $T_C$, the electronic parts of the thermal conductivities are close to each other in all alloys studied.

## I. INTRODUCTION

Development of a consistent, first-principles transport theory is a long-standing problem in the theory of metals and alloys. In disordered alloys, depending on composition and the chemical types of the alloying elements, the electron mean free path (MFP) can be as large as hundreds of lattice parameters or as short as one (Table I). Consequently, the interpretation of charge or heat carriers in disordered alloys changes from well-defined long-lived quasiparticles [1] to excitations that fall outside the traditional quasiparticle description. In the latter case, transport is normally described by diffusive physics [2] and the traditional Boltzmann equation approach [1,3,4] is no longer applicable. On the other hand, the Kubo-Greenwood (KG) [5,6] approach to the calculation of the conductivity does not suffer from this problem [7] in that it deals directly with the current-current correlation function.

For disordered alloys, use of the Green's-function formulation of the KG expression makes it possible to perform the necessary configurational averages of the conductivity using the coherent-potential approximation (CPA) [8,9]. This approach has an advantage of preserving the analytic properties of the conductivity within the thermodynamic limit [10,11],

albeit at the expense of the use of mean-field CPA. Implemented in conjunction with multiple scattering and density functional theory (DFT) [12], the Korringa-Kohn-Rostoker coherent-potential approximation (KKR-CPA) [13] provides a fully *ab initio* approach to calculating transport coefficients of disordered alloys. In contrast to KKR-CPA, a recently developed approach uses DFT supercell calculations to directly evaluate the KG expression [14–16]. However, for disordered alloys, configurational averaging and the thermodynamic limit must be done by hand. A similar situation pertains to another direct approach based on the results of time-dependent DFT that has been proposed and tested in the case of aluminum by Andrade, Hamel, and Correa [17].

Initially, the KKR-CPA approach was applied to the calculation of residual resistivity where electron scattering is caused by "chemical" disorder only [11,18]. This parameter-free approach leads to a very good agreement with experimental data [19] for nonmagnetic metals. Later, the developed approach was extended to incorporate electron scattering on lattice vibrations [20,21] and magnetic moment fluctuations [22,23] within the alloy analogy model. A similar approach was used to calculate electric, thermoelectric, and thermal transport properties of CoFe alloys based on the Kubo linear response formalism [24].

In the current paper, this approach was applied to the calculation of electrical and thermal conductivity in fcc concentrated solid solutions of the 3*d*-transition metals Ni,

*Corresponding author: samolyukgd@ornl.gov

TABLE I. Calculated majority (UP) spin states' density of states (total in the case of nonmagnetic $Ni_{0.8}Cr_{0.2}$ and $Ni_{0.33}Co_{0.33}Cr_{0.33}$) $N(E_F)$, Fermi velocities $\sqrt{\langle v_x^2 \rangle}$, experimental [28] residual resistivity, calculated electron mean free path $l$, experimental lattice parameter [29], calculated magnetic moments of each component (separated by a slash), Curie temperatures $T_C$ both experimental [29] and calculated within GGA and LSDA approximation for the exchange-correlation energy, and calculated residual resistivity (both GGA and LSDA).

| | Ni | $Ni_{0.5}Co_{0.5}$ | $Ni_{0.5}Fe_{0.5}$ | $Ni_{0.33}Co_{0.33}Fe_{0.33}$ | $Ni_{0.8}Cr_{0.2}$ | $Ni_{0.33}Co_{0.33}Cr_{0.33}$ |
|---|---|---|---|---|---|---|
| $N(E_F)$ (UP) (states/hartree) | 4.3 | 2.0 | 4.0 | 3.0 | 45.13 | 44.05 |
| $\sqrt{v_x^2}$ (UP) ($10^6$ m/s) | 0.43 | 0.46 | 0.46 | 0.46 | 0.24 | 0.24 |
| Experimental $\rho$ ($\mu\Omega$ cm) | 0.1 | 2.07 | 10.37 | 4.87 | 77 | 93.21 |
| $l$ (UP) (Å) | 3595 | 1689 | 174 | 478 | 4.1 | 4.0 |
| $a$ (Å) | 3.524 | 3.5345 | 3.5825 | 3.569 | 3.595 | 3.559 |
| Magnetic moment $\mu_B$ | 0.56 | 0.62/1.64 | 0.63/2.54 | 0.63/1.57/2.42 | | |
| Experimental $T_C$ (K) | 628 | 1117 | 780 | 995 | | |
| Calculated $T_C$ (GGA/LDA) (K) | 342/298 | 1180/990 | 955/810 | 1180/1045 | | |
| Calculated $\rho$ (GGA/LDA) $\mu\Omega$ cm | | 0.7/0.9 [63] | 2.1/3.3 [63] | 1.9/2.9 [63] | 78.1/77.0 | 68.6/67.6 [63] |

Fe, Co, and Cr. This group of alloys, including the extreme case of high entropy alloys [25,26], demonstrates unusual transport properties [27–30]. Thus, the low-temperature ($T = 4$ K) resistivity in these alloys varies, for example, between 1.3 $\mu\Omega$ cm in $Ni_{0.5}Co_{0.5}$ and 124.8 $\mu\Omega$ cm in NiCoFeCrPd [29]. The resistivity of NiCoFeCrPd is within the Mott-Ioffe-Regel (MIR) limit [31]. The MFP in such conductors is comparable with the interatomic distances, and transport is normally described by diffusive physics. Electrical and thermal conductivities are calculated here for Ni, $Ni_{0.5}Co_{0.5}$, $Ni_{0.5}Fe_{0.5}$, $Ni_{0.33}Co_{0.33}Fe_{0.33}$, $Ni_{0.8}Cr_{0.2}$, and $Ni_{0.33}Co_{0.33}Cr_{0.33}$. The first three alloys in this group are typical representatives of low-resistivity alloys $\rho < 10\,\mu\Omega$ cm and the last two alloys typify high-resistivity ones, $\rho > 75\,\mu\Omega$ cm [27–29]. According to our estimations presented in Table I, the MFP value in these alloys varies from 1689 to 4 and the last value is comparable to the lattice parameter ($\sim$3.6 Å). A unique set of properties such as significant variation of the MFP with the alloy concentration, typical metallic number of current carriers at the Fermi energy (see Table I), almost perfect fcc lattice atomic positions, together with the fact that background properties of these alloys can be described within regular DFT [27] makes concentrated solid solutions of 3*d*-transition metals a perfect playground for the investigation of the electronic transport in general.

In Sec. II the approaches used to calculate electrical and thermal conductivities of alloys are presented together with experimental details of high-temperature resistivity measurements in $Ni_{0.33}Co_{0.33}Fe_{0.33}$ and $Ni_{0.35}Co_{0.35}Cr_{0.30}$. The calculated electronic structure and magnetic properties, including the temperature dependence of the magnetization and the Curie temperatures, are presented in Sec. III A. In Sec. III B we discuss the results for electrical and thermal conductivities and we finally conclude in Sec. IV.

## II. THEORETICAL APPROACHES, DETAILS OF CALCULATIONS, AND EXPERIMENTAL PROCEDURES

The linear response of a system to an electric field, $\vec{E}$, and (or) a temperature gradient, $\nabla T$, is characterized by electric current, $\vec{j}$, and energy flux, $\vec{j_q}$, densities and is described by the linear response equations [7]

$$e\vec{j} = e\mathcal{L}_{11}\vec{E} - \mathcal{L}_{12}\frac{\nabla T}{T},$$
$$e\vec{j_q} = e\mathcal{L}_{21}\vec{E} - \mathcal{L}_{22}\frac{\nabla T}{T}, \quad (1)$$

where $e$ is the electron charge. In the following formalism proposed by Chester and Thellung (see Refs. [32,33]) based on the Mott relations [34] the transport coefficients, $\mathcal{L}_{ij}$, can be expressed as follows:

$$\mathcal{L}_{ij}^{\alpha\alpha} = (-1)^{i+j}\int d\varepsilon\,\sigma_{\alpha\alpha}(\varepsilon)(\varepsilon - \mu)^{i+j-2}\left[-\frac{\partial f(\varepsilon)}{\partial\varepsilon}\right], \quad (2)$$

where $\mu$ is the chemical potential, $-\partial f(\varepsilon)/\partial\varepsilon$ is the derivative of the Fermi distribution function, and $\alpha$ is the Cartesian index. The above relationships may be applied to each spin channel separately. This approximation is valid in the limit of weak spin-orbit coupling as is the case for the fcc 3*d*-transition-metal alloys that are the subject of this paper. $\sigma_{\alpha\alpha}(\varepsilon)$ is calculated using the Kubo-Greenwood [5,6] expression for the static conductivity,

$$\sigma_{\alpha\alpha}(\varepsilon) = \frac{\pi\hbar}{V}\left\langle\sum_{a,b}|\langle a|\hat{j}_\alpha|b\rangle|^2\delta(\varepsilon_a - \varepsilon)\delta(\varepsilon_b - \varepsilon)\right\rangle, \quad (3)$$

where $\hat{j}_\alpha$ is the current operator. The quantum states $|a\rangle$ in Eq. (4) represent the exact eigenfunctions of a particular configuration of the random potential, and the large angle brackets indicate an average over configurations.

The expression for the static conductivity should be reformulated using a definition of the single-particle Green's function [10,11], $G$, as

$$\sigma_{\alpha\alpha}(\varepsilon) = -\frac{\hbar}{V\pi}Tr\langle\hat{j}_\alpha\mathrm{Im}G(\varepsilon + i0)\hat{j}_\alpha\mathrm{Im}G(\varepsilon + i0)\rangle. \quad (4)$$

This expression allows one to calculate transport coefficients in disordered alloys by applying the CPA [8,9] and multiple scattering theory [13]. Details of the static conductivity calculation procedure can be found in Butler [11] and Butler and Stocks [18].

This approach allows one to calculate the temperature dependence of both the electrical conductivity,

$$\sigma_{\alpha\alpha}(T) = \mathcal{L}_{11}^{\alpha\alpha} = \int d\varepsilon \, \sigma_{\alpha\alpha}(\varepsilon) \left( -\frac{\partial f(\varepsilon, T)}{\partial \varepsilon} \right), \quad (5)$$

and the electronic part of the thermal conductivity:

$$e^2 T \kappa_{\alpha\alpha}(T) = \mathcal{L}_{22}^{\alpha\alpha} - \frac{\mathcal{L}_{21}^{\alpha\alpha} \mathcal{L}_{12}^{\alpha\alpha}}{\mathcal{L}_{11}^{\alpha\alpha}}. \quad (6)$$

Following Sommerfeld, expression (6) can be expanded to the second order in $k_B T/\mu$,

$$\kappa(T) \cong \frac{1}{3} \left( \frac{\pi}{e} \right)^2 k_B^2 T \left\{ \sigma(\mu) - \frac{[\pi k_B T \sigma'(\mu)]^2 / 6}{\sigma(\mu) + (\pi k_B T)^2 \sigma''(\mu)/6} \right\}, \quad (7)$$

where $\sigma'(\mu)$ and $\sigma''(\mu)$ are the first and second energy derivatives of the static electrical conductivity. The zeroth-order $k_B T/\mu$ contribution in Eq. (7) corresponds to the Wiedemann-Franz (WF) law.

Since the chemical potential, $\mu$, in transition metals is comparable to the width of the $d$ band ($\sim$5 eV in 3$d$ metals) and we focus on intermediate temperatures ($\theta_D \leqslant T \leqslant 3\theta_D$, where $\theta_D$ is the Debye temperature, which is $\sim$400 K for the alloys discussed in the text), the condition $k_B T/\mu \ll 1$ is satisfied, and Eq. (7) is applicable if the two first derivatives of $\sigma(\mu)$ are defined. The deviation from the WF law at low temperatures caused by nonelastic scattering or the presence of additional gapless neutral collective degrees of freedom [35,36] is not a subject of the current investigation. However, the approach presented allows one to take into account details of the electronic structure such as a complicated Fermi surface, electronic bands with nontrivial momentum dependence, and broadening caused by different types of disorder including that induced by temperature.

The main contributions to the resistivity in magnetic alloys correspond to electron scattering caused by chemical disorder, magnetic moment fluctuations, and lattice vibrations. By using the alloy analogy model all three scattering processes are included in the CPA resistivity calculation on an equal footing [20–23]. The details of the approach used are given in a publication by Ebert *et al.* [37]. The electronic structure of the alloys was calculated using the fully relativistic SPR-KKR-CPA method [38,39] with the angular momentum cutoff $l_{max} = 3$. The resistivity was calculated with $l_{max} = 4$. The exchange-correlation energy was calculated using both generalized gradient approximation (GGA) with the parametrization by Perdew, Burke, and Ernzerhof (PBE) [40] and local spin-density approximation (LSDA) with the parametrization by Vosko, Wilk, and Nusair [41]. Hereafter, the results are obtained using the PBE exchange correlation if not specified otherwise. Mean-square atomic displacements at different temperatures were obtained using Debye's theory with a composition-averaged Debye temperature. Neutron-scattering measurements showed that the phonon dispersion in all discussed alloys is similar to that of nickel [42]. The convergence of the residual resistivity with respect to the Brillouin-zone (BZ) mesh is extremely sensitive to alloy composition and components. The details of the convergence testing for the case of $Ni_{0.5}Fe_{0.5}$ and $Ni_{0.5}Co_{0.5}$ alloys can be found in the

Supplemental Material [43]. According to our results, the BZ integration can be safely executed over $\sim$1.4$\times$10$^5 k$ points in low-resistivity alloys and $\sim$5$\times$10$^3 k$ points in high-resistivity alloys in the full BZ.

Magnetic ordering in the alloys was described by the classical Heisenberg model

$$\hat{H} = -\sum_{i,j; i \neq j} J_{ij} \vec{e}_i \vec{e}_j, \quad (8)$$

where $\vec{e}_i$ corresponds to the direction of the magnetic moment on atom $i$ and $J_{ij}$ is the exchange coupling parameter for the atom pair $(i, j)$. Within this model, magnetic moments are treated as rigid and the $J_{ij}$ are calculated using a linear response approach [44] in the ferromagnetic state. The averaged magnetic moments of alloy components as a function of temperature are calculated using the cluster field method (CFM) [45]. The CFM approach is equivalent [46] to the cluster-variation method [47,48] if the largest size of the clusters corresponds to pairs of atoms. It was shown [49] that the Curie temperature obtained within this approximation overestimates more accurate technique results (spin dynamics) by $\sim$10%.

The averaged electronic Fermi velocities $\langle v_x^2 \rangle = \langle \sum_{\vec{k}, \nu} v_x^2(\vec{k}, \nu) \delta(\varepsilon_{\vec{k}, \nu} - E_F) \rangle$ were calculated using tight-binding linear muffin-tin orbitals [50] and the CPA formalism [51,52]. The calculated velocities were used to estimate values of the MFP through the experimental resistivity, $\rho$, using the expression

$$l = \frac{3}{[\rho e^2 \langle v^2 \rangle^{1/2} N(E_F)]} \quad (9)$$

with electron charge, $e$, calculated electron velocity, $\langle v^2 \rangle^{1/2} = \sqrt{3} \langle v_x^2 \rangle^{1/2}$, and electronic density of states at the Fermi energy, $N(E_F)$. The corresponding values for these quantities are presented in Table I. The underlying structure symmetry-relation for the electron velocity was used in Eq. (9). In magnetic $Ni_{0.5}Co_{0.5}$, $Ni_{0.5}Fe_{0.5}$, and $Ni_{0.33}Co_{0.33}Fe_{0.33}$ alloys, the velocities and density of states of the majority-spin electrons were taken into account in the MFP calculations, since electrons in the minority-spin channel do not significantly contribute to the conductivity because of the large scattering in this channel.

The lattice thermal resistivity caused by phonon-phonon scattering in Ni metal and $Ni_{0.5}Co_{0.5}$ and $Ni_{0.5}Fe_{0.5}$ alloys was obtained from first-principles electronic structure calculations combined with the conventional Boltzmann transport equation and the relaxation-time approximation. The thermal conductivity tensor is

$$\kappa_{\alpha\beta} = \frac{1}{V} \sum_\lambda \left( \partial n_\lambda^0 / \partial T \right) \hbar \omega_\lambda v_{\lambda\alpha} v_{\lambda\beta} \tau_{\lambda\alpha}, \quad (10)$$

where $V$ is the crystal volume, $\alpha$ and $\beta$ are Cartesian coordinates, $n_\lambda^0$ is the Bose factor, $\omega_\lambda$ is the phonon frequency for mode $\lambda$, $v_{\lambda\alpha}$ is the group velocity of phonon mode $\lambda$, and $\tau_{\lambda\alpha}$ is the phonon lifetime (inverse of the scattering rate) obtained from *ab initio* calculations of the phonon-phonon scattering rate (see more details in Refs. [53,54]). The lattice thermal conductivities—due to phonon-phonon scattering—are then calculated using the ShengBTE package [55]. To account for the disordered environment in alloys, the virtual crystal

approximation (VCA) was employed. This approximation does not include phonon scattering resulting from mass or force disorder (see discussion). The harmonic force constants were estimated using density functional perturbation theory (DFTP) as implemented in QUANTUM ESPRESSO (QE) [56]. In addition, third-order force constants were evaluated based on a 64-atom rhombohedral unit cell using the *ab initio* finite difference method in QE. PBE parametrization is used for exchange and correlation in all calculations. The ultrasoft pseudopotential [57] was employed with the plane-wave cut-off equal to 32 Ry. The BZ integration was performed using $\gamma$-center $16 \times 16 \times 16$ ($2 \times 2 \times 2$) $k$-point meshes for primitive cell DFPT [58,59] calculations and supercell calculations, respectively.

The electrical resistivity of $Ni_{0.33}Co_{0.33}Fe_{0.33}$ and $Ni_{0.35}Co_{0.35}Cr_{0.3}$ was measured to approximately 1060 K using a four-point configuration [60] with platinum wires spot welded to the samples. Currents of 0.5 and 1.0 mA were employed with alternating bias direction for the measurements of $Ni_{0.35}Co_{0.35}Cr_{0.3}$ and $Ni_{0.33}Co_{0.33}Fe_{0.33}$, respectively. The temperature was monitored with two type-E thermocouples and an average value is reported; the measurements were performed in an argon atmosphere. The data were collected using a Keithley 220 current source and a Keithley 2182 nanovoltmeter with facilitation by a PYTHON code. In these resistivity measurements the samples were a single crystal. The composition of the experimental $Ni_{0.35}Co_{0.35}Cr_{0.3}$ sample is slightly different from the one used in theoretical calculations, $Ni_{0.33}Co_{0.33}Cr_{0.33}$, but, according to calculations, this small difference in concentration modifies the residual resistivity by no more than 2%.

## III. RESULTS AND DISCUSSION

### A. Electronic structure and magnetic properties

The investigated concentrated solid solutions are naturally separated into two groups—alloys in one group contain Cr (typical representatives are $Ni_{0.8}Cr_{0.2}$ and $Ni_{0.33}Co_{0.33}Cr_{0.33}$) and alloys from the second group do not. It should be mentioned that, despite the fact that the use of DFT is in general well justified for such systems, self-consistent calculations of $Ni_{0.33}Co_{0.33}Cr_{0.33}$ converged to a magnetic ground state, in both supercell and CPA approaches, while experimentally this alloy is nonmagnetic. In addition, $NiCoCr_x$ exhibits quantum critical behavior near $x = 0.8$ [61].

To be consistent with experimental results, the $Ni_{0.33}Co_{0.33}Cr_{0.33}$ alloy was treated in our calculations as nonmagnetic. The details of the electronic structure of the group of alloys were discussed in our previous publications [27,62,63]. For the convenience of the readers, the discussion is reproduced for $Ni_{0.5}Co_{0.5}$ and $Ni_{0.8}Cr_{0.2}$. The spin-resolved electronic density of states (DOS) are shown in Figs. 1(a) and 1(b) for Co and Cr containing alloys, respectively (DOS for the other alloys can be found in the Supplemental Material [43]). In the figure, the Fermi energy is taken as zero. For each alloy panel, the left (right) panels correspond to the DOS of majority-spin (minority-spin) states. Within each panel, the solid red (dashed blue) lines correspond to the Ni (second-species) local DOS. Similarly,
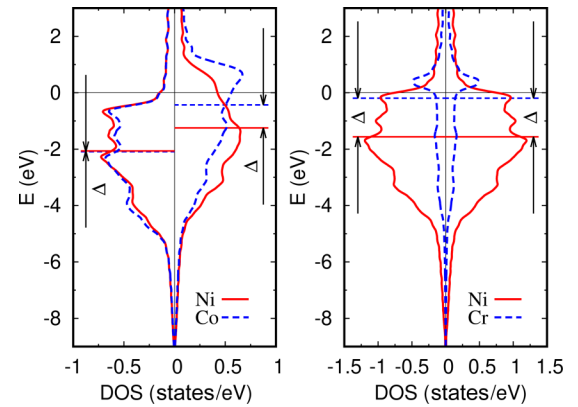


FIG. 1. Projected density of states of magnetic NiCo (left) and nonmagnetic $Ni_{0.8}Cr_{0.2}$ (right) shown by dashed blue lines for Co/Cr and a solid red line for Ni atoms. The Fermi energy corresponds to zero on the vertical axis. The centers of the $d$ bands are shown by horizontal lines, where splitting is denoted by $\Delta$.

the horizontal solid red (dashed blue) lines denote the centers of gravity of the Ni (second-species) spin-resolved $d$-band center of the corresponding species. It equals the resonance energy $E_d$ of the $d$-wave (angular momentum channel $l = 2$) scattering phase shift $\delta_d$, i.e., the energy satisfying the conditions $\delta_d(E_d) = \pi/2$ (see discussion in our previous publications [62,63]). A Cr atom contains five $d$ electrons and has a half-filled $d$ band whereas Fe, Co, and Ni belong to the group of transition metals with an almost filled $d$ band. This results in different magnetic exchange coupling—3$d$-transition metals with almost filled $d$ bands have a tendency to ferromagnetic ordering, while metals with half-filled bands tend to exhibit antiferromagnetic ordering [64,65]. Additionally, the electronic structure of metals from these two groups behave differently upon alloying. The occupation of $d$ bands and the resulting position of the Fermi level can be approximately obtained by minimization of the band-structure energy, $E_b$, together with additional constraints to preserve atomic charge neutrality. In alloys with a similar number of $d$ electrons (Fe, Co, Ni) $E_b$ minimization results in the alignment of majority-spin $d$ states, e.g., in $Ni_{0.5}Co_{0.5}$ with almost negligible splitting, $\Delta$, between Ni and Co $d$-band centers ($\Delta/W \ll 1$, where $W$ is the $d$ bandwidth). This corresponds to weak scattering in the majority-spin channel and a low resistivity in this channel. This weak scattering creates a "shortcut" for the electrical current resulting in a small total residual resistivity typical for high conductivity alloys. The scattering in the minority-spin channel can be estimated from the relation between exchange splitting and the size of the magnetic moment of each element [62]. The large difference in the number of $d$ electrons in Cr and Ni does not allow alignment of the $d$ bands of each component while preserving atomic charge neutrality. Together with an absence of spin polarization, this results in a large $d$-band splitting $\Delta = 0.73$ eV in both spin channels with significant electron scattering and, as a result, a large residual resistivity. These conclusions agree with experimental observations [27,29] that all compounds containing Cr belong to the low conductivity group. This analysis can easily be extended to alloys containing more than two components [63].

Important information about the character of electron dynamics in an alloy can be obtained from the values of the MFP. In the current publication the MFP was estimated from the resistivity using Eq. (9). Since the main channel for electron propagation in magnetic alloys corresponds to majority-spin states, the corresponding Fermi velocity, $\langle v_x^2(E_F) \rangle^{1/2}$, and density of states, $N(E_F)$, are used in Eq. (9). In magnetic alloys, the electronic states at the Fermi level in the majority-spin channel correspond to $sp$ electrons [see Fig. 1(a)] with a high velocity of $0.46 \times 10^6$ m/s (Table I) that is only weakly dependent on the chemical composition, whereas in nonmagnetic Cr containing alloys the electronic states correspond to $d$ electrons with low-energy dispersion [see Fig. 1(b)] and the corresponding velocities are almost a factor of 2 lower ($0.24 \times 10^6$ m/s) than in magnetic alloys. The MFP calculated for $Ni_{0.5}Co_{0.5}$ equals 1690 Å and is comparable to the values for pure transition metals, which is not surprising since the electronic structure of a $Ni_{0.5}Co_{0.5}$ alloy can be described within the VCA with high accuracy [27,62]. The MFPs in $Ni_{0.5}Fe_{0.5}$ and $Ni_{0.33}Co_{0.33}Fe_{0.33}$ are significantly smaller, 174 and 478 Å, respectively. However, in all three of these alloys, the calculated MFP is significantly larger than the lattice parameter of ∼3.6 Å, and consequently electronic transport in the alloys containing all components with almost filled $d$-electron states can be interpreted as a propagation of well-defined quasiparticles obeying the Boltzmann equation [66–68]. In contrast to this group of alloys, the presence of Cr dramatically increases electron scattering and reduces the MFP to values equal to 4.1 and 4.0 Å in $Ni_{0.8}Cr_{0.2}$ and $Ni_{0.33}Co_{0.33}Cr_{0.33}$, respectively. These values are comparable with the lattice parameter and hence the applicability of the Boltzmann equation to electron transport in these alloys is questionable. As we mentioned in the Introduction, the KG formalism allows one to calculate both the electronic and thermal conductivity without such limitations. For convenience of the readers, the calculated results for residual resistivity, already published by Mu *et al.* [63], are reproduced in Table I. As can be seen for the case of iron containing alloys, the LSDA result is ∼30% larger than the GGA one. For the rest of the alloys LSDA and GGA results are close to each other. Detailed discussion of residual resistivity results and comparison with experiment can be found in Ref. [63].

In the magnetic alloys the contribution of electron scattering by temperature-dependent magnetic moment fluctuations to the electrical and thermal conductivity was calculated using the Heisenberg model, Eq. (8), and the averaged value of the magnetic moment as a function of temperature. The calculated zero-temperature values of the magnetic moments are weakly dependent on alloy composition and are approximately $0.6\mu_B$, $1.6\mu_B$, and $2.5\mu_B$ for Ni, Co, and Fe, respectively (Table I). The range of the calculated exchange couplings, $J_{ij}$, in alloys does not exceed 1.8 lattice parameters (see Supplemental Material [43]) and 2.0 lattice parameters in pure Ni. In the current calculations, all atomic magnetic moments were treated as rigid vectors and the well-known longitudinal fluctuations of Ni [69,70] were not taken into account. This results in a significantly underestimated Curie temperature, $T_C$, for pure Ni [44,64] of 342 K, calculated using the PBE parametrization of the exchange-correlation energy versus the experimental value of 628 K. Below, for
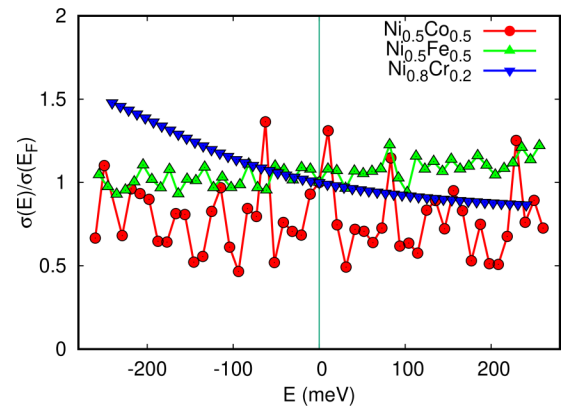


FIG. 2. Static electrical conductivity as a function of energy calculated in three alloys. The Fermi energy corresponds to zero.

the calculation of the conductivity, the temperature dependence of the magnetization for pure Ni was rescaled by the experimental Curie temperature. In the alloys the dominant magnetic interaction corresponds to Fe or Co atoms. For these elements, the rigid spin approximation is a very reasonable approach [69] and the calculated Curie temperatures are in much better agreement with experiment. The Curie temperatures were overestimated by 6% in $Ni_{0.5}Co_{0.5}$ and by 20% in $Ni_{0.5}Fe_{0.5}$ and $Ni_{0.33}Co_{0.33}Fe_{0.33}$ alloys. Curie temperatures obtained within LSDA are 10–20% lower compared to GGA PBE ones. The calculated magnetic transition in all alloys is of second order.

### B. Results for transport properties

The electronic part of the alloy thermal conductivity is calculated using Eq. (6), where the transport coefficients $\mathcal{L}_{ij}^{\alpha\alpha}$ are obtained through integration over energy of the static conductivity and the derivative of the Fermi distribution function, Eq. (2). At low temperatures the approximate Eq. (7) is used. A necessary condition for the application of expression (7) for the thermal conductivity is that it is "well behaved" on an energy scale of the half width of the derivative of the Fermi function at temperature $T$. In Fig. 2 the energy dependence of zero temperature $\sigma(E)$ is presented for $Ni_{0.5}Co_{0.5}$, $Ni_{0.5}Fe_{0.5}$, and $Ni_{0.8}Cr_{0.2}$. Because of large scattering in both spin channels, $\sigma(E)$ in $Ni_{0.8}Cr_{0.2}$ is a smooth function, while, for $Ni_{0.5}Co_{0.5}$ and $Ni_{0.5}Fe_{0.5}$, $\sigma(E)$ changes nonmonotonically near the Fermi energy. Such a behavior is caused by the Ni, Co, and Fe majority-spin state alignment as discussed above in the text. As a result, electron scattering in this spin channel is weak and electron excitations are well-defined long-living quasiparticles described by "zero" thickness bands. This results in the presence of fine structure in the electronic density of states around the Fermi energy, which is dominated by $d$ states. In these alloys the applicability of Eq. (7) is questionable. However, $\sigma(E)$ in Eqs. (6) and (7) should be calculated at some particular temperature and should include the effects of electron scattering on the temperature-induced magnetic moment fluctuations as well as lattice vibrations. After incorporation of scattering on just magnetic moment fluctuations, the character of the conductivity energy dependence changes dramatically
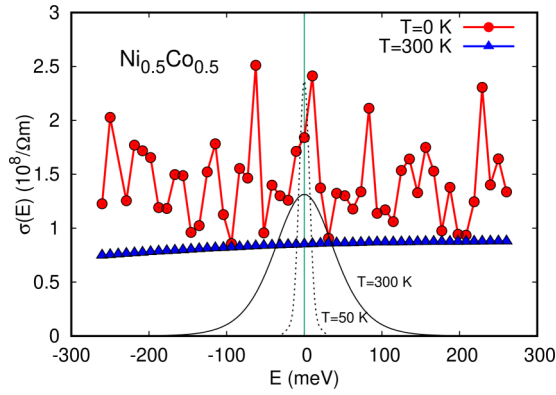
FIG. 3. Electrical conductivity in $Ni_{0.5}Co_{0.5}$ as a function of energy calculated with magnetic moment fluctuation at temperature $T = 300$ K (blue line with triangles) and with perfect magnetic ordering (red line with circles). The derivative of the Fermi distribution function $(-\partial f/\partial E)$ is shown by black solid ($T = 300$ K) and dashed ($T = 50$ K) lines in relative units.

(see Fig. 3). In $Ni_{0.5}Co_{0.5}$ this dependence changes from a set of sharp peaks to a slowly monotonically growing function. Thus, even in the worst case of $Ni_{0.5}Co_{0.5}$ Eq. (7) is applicable and is used in our calculations.

### 1. Results for pure Ni

The results for the resistivity of pure Ni are consistent with previously published ones [37]. Below the Curie temperature the calculated resistivity, shown by a red solid line with filled circles in Fig. 4(a), systematically overestimates the experimental values [28] by $\sim 10\,\mu\Omega$ cm. The reason for this difference is a discrepancy between the experimental temperature dependence of the magnetization and the magnetization calculated from the classical Heisenberg model. The calculated magnetization decreases with temperature faster than the experimental magnetization [71] [inset in Fig. 4(a)], and, as a result, electron scattering on magnetic moment fluctuations is overestimated. To prove this statement, the experimental temperature dependence [71] is also used to calculate the resistivity (shown by a green line with filled down triangles). The deviation from the experimental results in this case is below 15% for temperatures up to 400 K. As the temperature approaches $T_C$ the deviation from experiment doubles in both types of calculations. This deviation is a result of the rigid magnetic moment used in our calculation. The electron scattering by fluctuations of fully disordered magnetic moments of $0.6\mu_B$ is significantly larger than the moment fluctuations of $0.3-0.4\mu_B$ experimentally observed near the Curie temperature (see Ref. [72] and references therein).

Following Ebert *et al.* [37], above the Curie temperature the resistivity is calculated in the nonmagnetic state. The resistivity in this case is defined by electron scattering on lattice vibrations only. The calculated resistivity is in perfect agreement with experiment above $T_C$.

The electronic part of the thermal conductivity calculated from the zeroth-order $(k_B T/\mu)$ term in Eq. (7) (corresponding to the WF law) and the theoretical magnetization is shown by
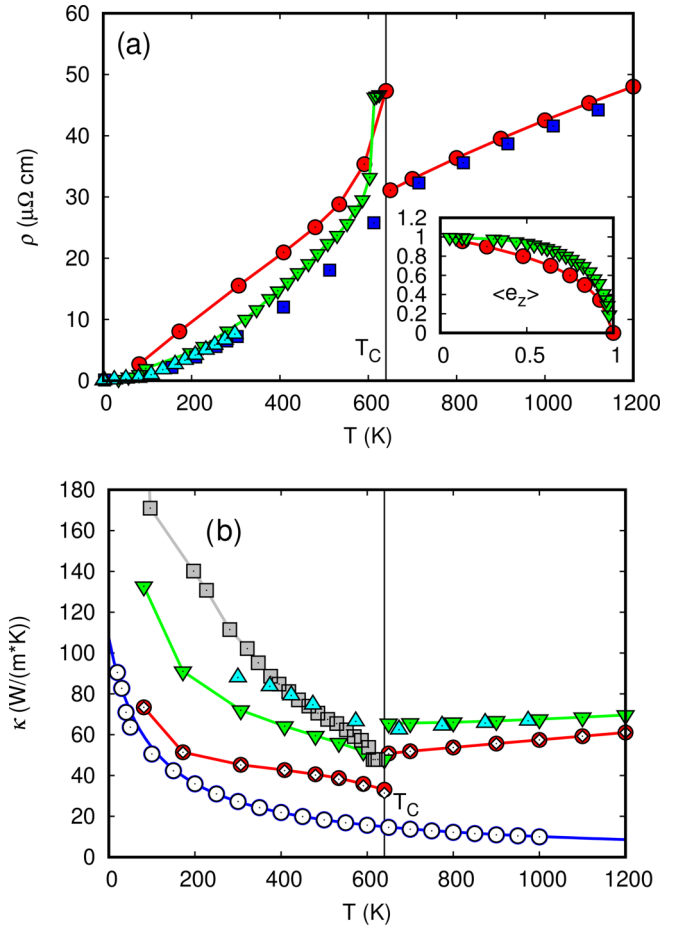


FIG. 4. (a) Electrical resistivity in Ni as a function of temperature calculated using CFM results for the magnetization (red line with filled circles) and experimental magnetization (green down triangles); the experimental resistivity is shown by cyan triangles [28] and blue squares [75]. Both experimental (green down triangles) and calculated (red circles) magnetization dependences of $T/T_C$ are shown in the inset. (b) Thermal conductivity, $\kappa$, as a function of temperature calculated using Eq. (7) and theoretical results for magnetization (the WF law result is shown by a red line with filled circles; the result with correction to the WF law is shown by empty diamonds). The lattice contribution to $\kappa$ is shown as a blue line with open circles. Total $\kappa$ calculated using theoretical magnetization is shown as a green line with down triangles, whereas that calculated using experimental magnetization is shown as a gray line with filled squares; experiment [29] is shown as cyan triangles. The experimental $T_C$ is indicated by a vertical line. All the calculated dependencies include scattering on both lattice vibrations and magnetic moment fluctuations.

a red line with filled circles in Fig. 4(b). The full calculated electronic $\kappa$, including second-order $(k_B T/\mu)$ corrections, is shown by empty diamonds. The derivatives of $\sigma(E)$ used in Eq. (7) were calculated numerically. As can be seen, there is no visual difference between these two sets of data at most temperatures, except a few percent deviations from WF at temperatures between 550 K and $T_C$. The lattice contribution to the thermal conductivity is shown by a blue line with open circles. Its temperature dependence could be approximately described by a power law, $1/T^\alpha$, where $\alpha = 0.97$, close to 1. This behavior of the lattice thermal conductivity

is very typical for ordered materials with the main source of phonon scattering coming from the three-phonon interaction. The total thermal conductivity is shown by a green line with filled down triangles. The calculated thermal conductivity above $T_C$ is in excellent agreement with experiment. This is not surprising since the calculated resistivity reproduces the experiment with high accuracy. Below the Curie temperature, the calculated thermal conductivity is underestimated by $\sim 20$ W/(m K). This is the result of the overestimated electrical resistivity. The total thermal conductivity calculated using the electronic part of the conductivity obtained from experimental magnetization data [green triangles in Fig. 4(a)] is shown by a gray line with filled squares. Similar to the resistivity case, incorporation of the experimental temperature dependence of the magnetization significantly improves agreement with experiment for all temperature regions except the interval between 550 K and $T_C$, where the longitudinal nickel magnetic moment fluctuations play an important role.

### 2. Results for ferromagnetic Ni₀.₅Co₀.₅, Ni₀.₅Fe₀.₅, and Ni₀.₃₃Co₀.₃₃Fe₀.₃₃

Results of resistivity calculations for $Ni_{0.5}Co_{0.5}$ alloys are presented in Fig. 5(a). The magnetization as a function of temperature for both alloy components was calculated by solving the classical Heisenberg model within the CFM approach. Similar to the case of nickel, this approach overestimates the rate of magnetization reduction with the temperature increase as compared to experiment. This results in an overestimation of the calculated resistivity compared to available experimental data [28]. Cobalt is the main magnetic component in this alloy. The longitudinal fluctuations of the Co magnetic moment are much smaller compared to nickel [68] and hence the rigid moment approximation used in the calculations is justified. Thus in the temperature interval between 200 K below and above $T_C$ much better agreement between the calculated resistivity and experiment is expected. This expectation is supported by very good agreement between the calculated and experimental thermal conductivity [29] in this interval of temperatures as shown in Fig. 5(b) by a green line with down triangles for the calculated result and up cyan triangles for the experiment. Results for the calculated lattice contribution were obtained within the VCA, which has limited applicability. It includes three-phonon scattering only and neglects phonon scattering on lattice disorder introduced by a random distribution of different types of atoms in the alloy. As was shown by Alam and Mookerjee [73], the temperature dependence of the lattice thermal conductivity, defined by phonon scattering on lattice disorder, is very different from the three-phonon scattering result. The alloy lattice thermal conductivity starts from zero at low temperatures and monotonically increases with the temperature until saturation is reached. However, above $2\theta_D$ three-phonon scattering dominates. At these temperatures, the VCA can be used to estimate the lattice thermal conductivity, and as can be seen from Fig. 5(b) at these temperatures there is reasonable agreement between theory (green line with down triangles) and experiment (cyan up triangles).
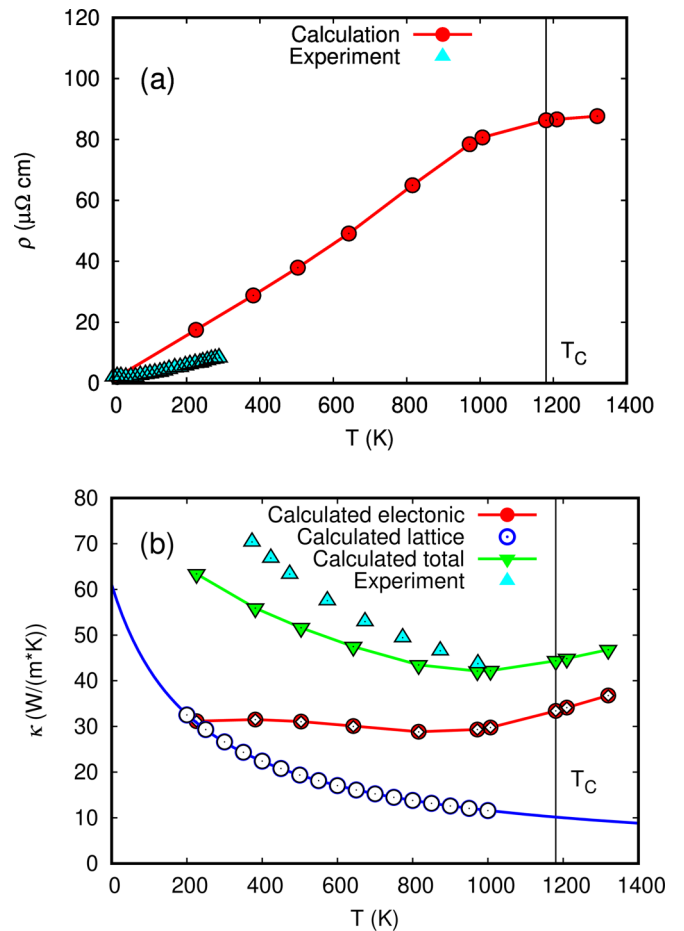


FIG. 5. (a) Electrical resistivity and (b) thermal conductivity in $Ni_{0.5}Co_{0.5}$. For notations see Fig. 4. In addition to the contribution from electron scattering on lattice vibrations and magnetic moment fluctuations, the result presented by a red line with filled circles contains a contribution from scattering on chemical disorder. The calculated $T_C$ is indicated by a vertical line.

Results for the calculated resistivity in $Ni_{0.5}Fe_{0.5}$ and $Ni_{0.33}Co_{0.33}Fe_{0.33}$ are very similar to the results obtained for $Ni_{0.5}Co_{0.5}$. It has a nonzero value at zero temperature, corresponding to the residual resistivity, caused by electron scattering on the chemical disorder. Because of majority-spin states alignment, as discussed in the previous section, the scattering in this channel is small and the residual resistivity is below $10 \, \mu\Omega$ cm—a value typical for low-resistivity alloys. As temperature increases, the resistivity increases with approximately the same rate and reaches $\sim 100 \, \mu\Omega$ cm at the Curie temperature, which is between 900 and 1150 K for all three alloys. The rapid increase of resistivity for temperatures below the Curie temperature is determined by increased scattering by magnetic fluctuations. Above the Curie temperature, the magnetic moment disorder reaches saturation when the averaged projection of the magnetic moment to the $z$ direction equals zero and the strength of electron scattering on magnetic moment fluctuations also saturates. The temperature dependence of the resistivity above $T_C$ is determined by the electron scattering on lattice vibrations, which grows linearly with temperature. As a result, above $T_C$ the resistivity slowly

rises with temperature. It is worthwhile to mention that the highest values of resistivity are close to the MIR limit. In the limit the electron mean free path is comparable to an interatomic spacing and the resistivity reaches saturation. However, this resistivity saturation has never been reached in both calculations and high-temperature experiments for $Ni_{0.33}Co_{0.33}Fe_{0.33}$, as shown by cyan triangles in Fig. 7(a). The low-temperature experimental data (below 300 K) are taken from Ref. [28], while data above 300 K have been obtained in the current paper. Agreement between experiment and theory is reasonably good. Thus around the Curie temperature the calculations reproduce the experimental resistivity with a few percent accuracy. At temperatures below 700 K deviation from experiment is more significant. The calculated resistivity increases with temperature much faster at low temperatures compared to experiment. Similar to nickel, this inconsistency is a result of the overestimated rate of magnetic moment projection reduction with the temperature increase as calculated by solving the classical Heisenberg model. Surprisingly, the calculated resistivity in $Ni_{0.5}Fe_{0.5}$ at temperatures between 200 and 400 K is in much better agreement with experiment, Fig. 6(a), than in $Ni_{0.5}Co_{0.5}$ and $Ni_{0.33}Co_{0.33}Fe_{0.33}$. This difference is caused by the much larger discrepancy between calculated, $2.45\,\mu\Omega\,cm$, and experimental, $10.37\,\mu\Omega\,cm$), residual resistivities (see Table I). As a result, although the calculated resistivity rises faster than the experimental one, due to its smaller-zero temperature value, the calculated resistivity begins to be very close to the experimental one at approximately 200 K and above. The difference between calculated and experimental residual resistivities is discussed in detail in Mu *et al.* [63].

The thermal conductivity temperature dependence is also very similar in all three alloys. It starts from values $50-65$ W/(m K) at approximately 200 K and monotonically decreases until reaching values $30-45$ W/(m K) at temperature $T'$ approximately 200 K below $T_C$. This decrease is a result of the increase in electron scattering by magnetic moment fluctuations and lattice vibrations with increasing temperature, the scattering strength grows faster than the number of heat carriers, which is proportional to temperature [$T$ coefficient in Eq. (8)]. Above $T'$ the thermal conductivity behavior changes and begins to increase with increasing temperature. This change in behavior is caused by the increasing number of heat carriers, which overcomes the conductivity decrease caused by electron scattering. This is primarily because scattering by magnetic moment fluctuations saturates. Similar to $Ni_{0.5}Co_{0.5}$ the correction to the WF law, shown by white diamonds in Figs. 6(b) and 7(b), can be neglected. However, in contrast to the $Ni_{0.5}Co_{0.5}$ alloy, the calculated thermal conductivity in $Ni_{0.5}Fe_{0.5}$ is overestimated by approximately 20% at temperatures above $2\theta_D$. For $Ni_{0.33}Co_{0.33}Fe_{0.33}$ the calculated thermal conductivity behaves like the averaged value of the $Ni_{0.5}Co_{0.5}$ and $Ni_{0.5}Fe_{0.5}$ conductivities and is in surprisingly good agreement with experiment.

Further, the experimental resistivity was used to calculate the electronic part of the thermal conductivity by applying the WF law and this was used as an input for the total thermal conductivity. The result is shown by gray squares in Fig. 7(b). As can be seen, the agreement with experiment is not as good as for the conductivity obtained from the calculated
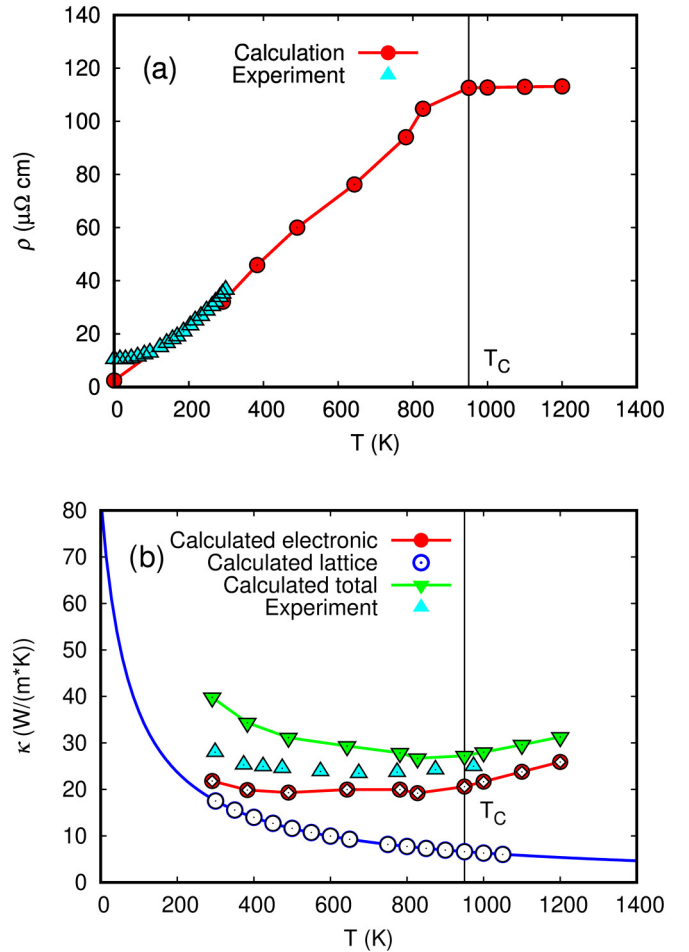


FIG. 6. (a) Electrical resistivity and (b) thermal conductivity in $Ni_{0.5}Fe_{0.5}$. For notations see Fig. 4. In addition to the contribution from electron scattering on lattice vibrations and magnetic moment fluctuations, the result represented by a red line with filled circles contains a contribution from scattering on chemical disorder. The calculated $T_C$ is indicated by a vertical line.

magnetization. The total $\kappa$ deviates from the experimental data below 700 K and this deviation increases with temperature reduction. Since, as was demonstrated above, the deviations from the WF law are negligible, the source of this disagreement should be attributed to an overestimated lattice thermal conductivity calculated within the VCA.

### 3. Results for nonmagnetic $Ni_{0.8}Cr_{0.2}$ and $Ni_{0.33}Co_{0.33}Cr_{0.33}$

The results for electrical resistivity in two representatives of high-resistivity alloys, $Ni_{0.8}Cr_{0.2}$ and $Ni_{0.33}Co_{0.33}Cr_{0.33}$, are presented in Figs. 8(a) and 9(a). Both alloys are nonmagnetic; consequently, the magnitude and temperature dependence of the conductivity is determined by electron scattering on chemical disorder and lattice vibrations only. As a result the temperature dependence of the electrical resistivity is much simpler. It starts from $\sim 80\,\mu\Omega\,cm$ (residual resistivity) and monotonically increases with the temperature [red line with filled dots in Figs. 8(a) and 9(a)]. The resistivity increase is slower in $Ni_{0.8}Cr_{0.2}$, by $7.8\,\mu\Omega\,cm$ for the temperature interval between 100 and 1200 K, than for $Ni_{0.33}Co_{0.33}Cr_{0.33}$, which increases
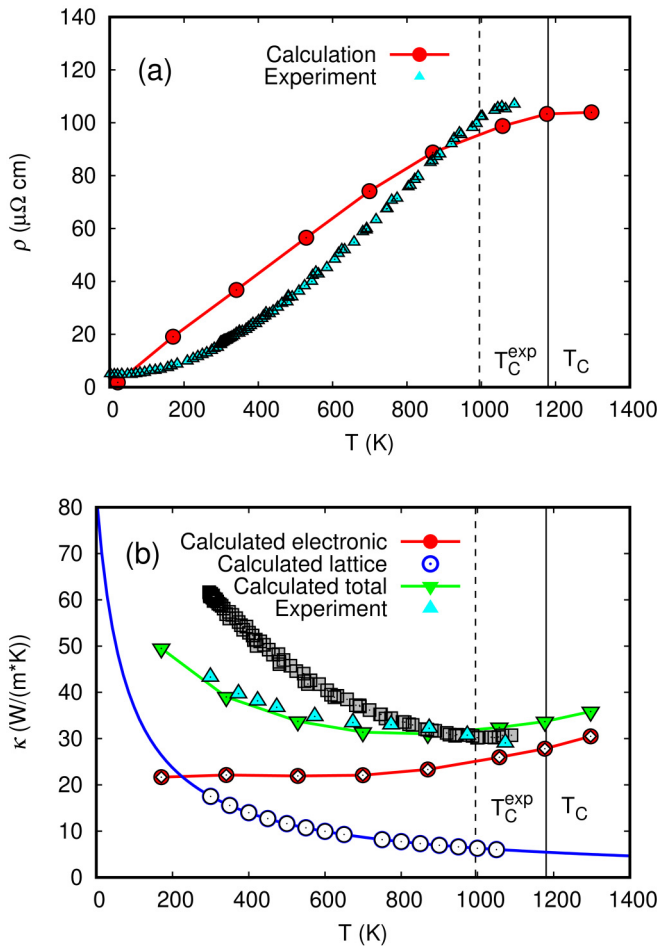
FIG. 7. (a) Electrical resistivity and (b) thermal conductivity in $Ni_{0.33}Co_{0.33}Fe_{0.33}$. For notations see Fig. 4. In addition to the contribution from electron scattering on lattice vibrations and magnetic moment fluctuations, the result represented by a red line with filled circles contains a contribution from scattering on chemical disorder. The total thermal conductivity calculated as a sum of lattice contribution and the electronic contribution obtained from experimental resistivity [cyan triangles in Fig. 7(a)] through the WF law is shown by gray color squares. The calculated, $T_C$, and experimental, $T_C^{exp}$, Curie temperatures are indicated by solid and dashed vertical lines, respectively.

by 16.6 $\mu\Omega$ cm over the same temperature interval. The slope of resistivity temperature dependence in $Ni_{0.33}Co_{0.33}Cr_{0.33}$ is slightly lower than the experimental slope as shown by triangles in Fig. 9(a). Also, the experimental slope slightly changes at 800 K. This transition is traditionally attributed to a K-state transition and it has been previously observed in experimental specific heat capacity measurements [29]. It should be mentioned that even while the resistivity starts at much higher values for low temperatures in Cr containing alloys—the so-called high-resistivity alloys—at about 1000 K the resistivity values are similar in all of the discussed solid solutions. In low-resistivity alloys the weak electron scattering on chemical disorder is compensated by electron scattering on magnetic moment fluctuations increasing with temperature.

The results for the thermal conductivity in these two alloys are presented in Figs. 8(b) and 9(b) by the filled red circles
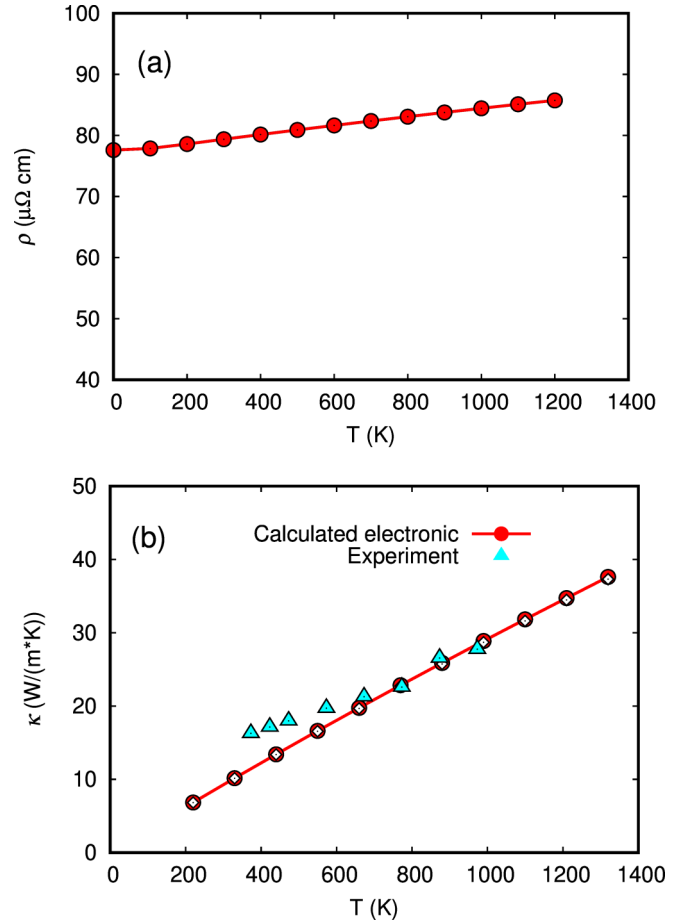


FIG. 8. (a) Electrical resistivity and (b) the electronic part of the thermal conductivity in $Ni_{0.8}Cr_{0.2}$. For notations see Fig. 4. The calculations have been done in the nonmagnetic state.

together with the correction to the WF law as shown by empty diamonds. Similar to the case of the low-resistivity alloys, there is no significant deviation from the WF law. In $Ni_{0.8}Cr_{0.2}$ the calculated electronic part of the thermal conductivity [Fig. 8(b)] is 5 W/(m K) lower than the experimental one at temperatures below 700 K, shown by blue triangles. Above 700 K, according to our results, the lattice contribution to the total conductivity equals zero. This result looks especially surprising taking into account the fact that traditionally it is supposed that in highly disordered systems the phonon contribution to the total thermal conductivity is larger than the electronic one [74]. The possible reason for this disagreement is an underestimated calculated resistivity. However, the absence of experimental data does not allow us to justify this assumption.

A similar result was obtained in $Ni_{0.33}Co_{0.33}Cr_{0.33}$ [Fig. 9(b)]. The calculated electronic part of the thermal conductivity, shown by a red line with filled circles, equals the total experimental conductivity at 600 K and below, slightly larger than the experiment above this temperature. The reason for this discrepancy is that the calculated electrical resistivity is approximately 10 $\mu\Omega$ cm lower than the experimental one [Fig. 9(a)]. The electronic part of the thermal conductivity calculated from the experimental electrical resistivity using
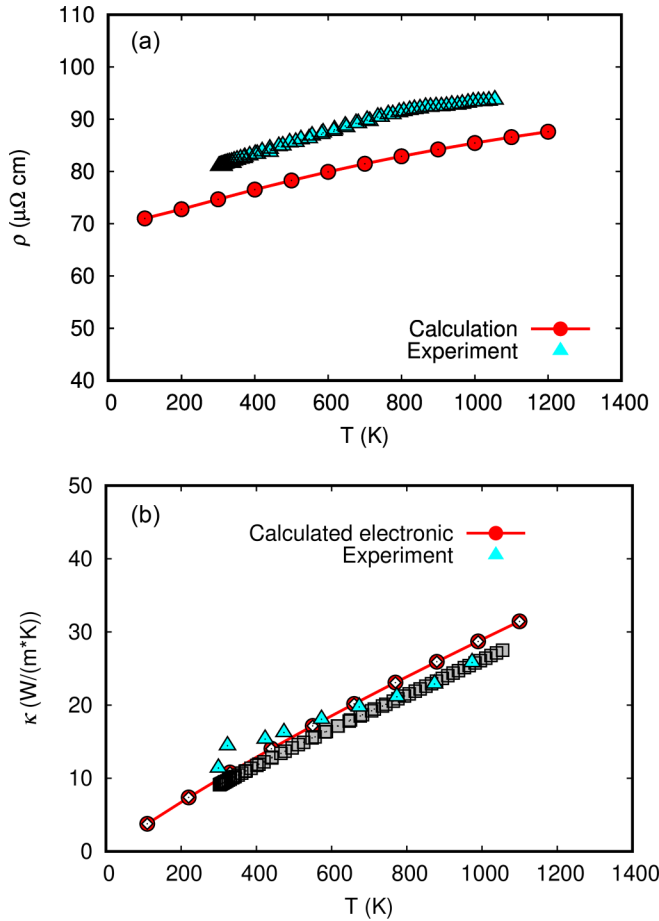
FIG. 9. (a) Electrical resistivity and (b) the electronic part of the thermal conductivity in $Ni_{0.33}Co_{0.33}Cr_{0.33}$. For notations see Fig. 4. The calculations have been done in the nonmagnetic state. The experimental resistivity obtained in the current paper for the compound $Ni_{0.35}Co_{0.35}Cr_{0.3}$ is shown as cyan color triangles. The electronic part of the thermal conductivity calculated from the experimental resistivity [cyan triangles in Fig. 9(a)] through the WF law is shown as gray color squares.

the WF law [gray squares in Fig. 9(b)] is in better agreement with experiment. In all intervals of the temperature it is lower than the total experimental thermal conductivity. According to the calculations, the contribution from the lattice conductivity equals 5 W/(m K) at room temperature and is reduced to approximately 2 W/(m K) at the highest temperatures. However, similar to $Ni_{0.8}Cr_{0.2}$, the lattice contribution is unexpectedly small.

## IV. CONCLUSIONS

The formalism proposed by Chester and Thellung [32] for the calculation of transport coefficients of Mott relations was applied to the calculation of alloy transport properties—electrical resistivity and the electronic part of the thermal conductivity. The electrical conductivity is used as an input for the calculation of thermal transport properties. The electrical conductivity was calculated using the Kubo-Greenwood formalism where the coherent-potential approximation was applied to obtain the alloy Green's function. This approach allows for a consistent calculation of the properties of disordered alloys

using configurational averaging and the thermodynamic limit. All sources for electron scattering, i.e., chemical disorder and temperature induced magnetic moment fluctuations and lattice vibrations, are included in the CPA scheme on equal footing using the alloy analogy model. This allows one to take into account details of the electronic structure such as a complicated Fermi surface, electronic bands with nontrivial momentum dependence, and broadening caused by disorder. In the current paper this approach was applied to the calculation of transport properties of the series of fcc concentrated solid solutions of the $3d$-transition metals Ni, Fe, Co, and Cr. Reasonable agreement with experimental data was obtained. It was demonstrated that in all alloys in the temperature interval of $\theta_D \leqslant T \leqslant 3\theta_D$ the deviation from the Wiedemann-Franz law is insignificant. This is because of the smearing of features in the electronic structure by temperature-induced magnetic moment fluctuations and lattice vibrations.

For the nonmagnetic alloys, $Ni_{0.8}Cr_{0.2}$ and $Ni_{0.33}Co_{0.33}Cr_{0.3}$, the combined effect of chemical disorder and electron-phonon scattering results in a monotonic increase in the resistivity as a function of temperature starting from a large residual resistivity. For magnetic $Ni_{0.5}Co_{0.5}$, $Ni_{0.5}Fe_{0.5}$, and $Ni_{0.33}Fe_{0.33}Co_{0.33}$ alloys, the residual resistivity is small, but additional electron scattering from temperature induced magnetic moment fluctuations results in a rapid increase of the resistivity as a function of temperature. Above the Curie temperature the electron scattering by magnetic moment fluctuations saturates and the resistivity slowly increases due to electron-phonon scattering.

The electronic part of the thermal conductivity in nonmagnetic high-resistivity alloys $Ni_{0.8}Cr_{0.2}$ and $Ni_{0.33}Co_{0.33}Cr_{0.33}$ monotonically increases with temperature. This behavior is a result of competition between conductivity reduction caused by electron-phonon scattering and temperature induced increase of the number of heat carriers. In magnetic low-resistivity alloys, the presence of magnetic fluctuations results in a rapid reduction of the thermal conductivity until this reduction is overcome by an increasing number of carriers at temperatures slightly below the Curie temperature. Similar to the resistivity, above $T_C$ the electronic parts of the thermal conductivities are similar in all investigated alloys.

[1] J. M. Ziman, *Electrons and Phonons: The Theory of Transport Phenomena in Solids* (Oxford University Press, Oxford, 1960).

[2] S. A. Hartnoll, Nat. Phys. **11**, 54 (2015).

[3] P. B. Allen, Phys. Rev. B **17**, 3725 (1978).

[4] S. Y. Savrasov and D. Y. Savrasov, Phys. Rev. B **54**, 16487 (1996).

[5] R. Kubo, J. Phys. Soc. Jpn. **12**, 570 (1957).

[6] D. A. Greenwood, Proc. Phys. Soc. London **71**, 585 (1958).

[7] G. D. Mahan, *Physics of Solids and Liquids*, Many-Particle Physics (Springer, New York, 2000).

[8] P. Soven, Phys. Rev. **156**, 809 (1967).

[9] W. D. Taylor, Phys. Rev. **156**, 1017 (1967).

[10] B. Velicky, Phys. Rev. **184**, 614 (1969).

[11] W. H. Butler, Phys. Rev. B **31**, 3260 (1985).

[12] W. Kohn and L. J. Sham, Phys. Rev. **140**, A1133 (1965).

[13] G. M. Stocks, W. M. Temmerman, and B. L. Gyorffy, Phys. Rev. Lett. **41**, 339 (1978).

[14] V. Recoules and J.-P. Crocombette, Phys. Rev. B **72**, 104202 (2005).

[15] S. Mazevet, M. Torrent, V. Recoules, and F. Jollet, High Energy Density Phys. **6**, 84 (2010).

[16] M. Pozzo, M. P. Desjarlais, and D. Alfè, Phys. Rev. B **84**, 054203 (2011).

[17] X. Andrade, S. Hamel, and A. A. Correa, arXiv:1702.00411v1.

[18] W. H. Butler and G. M. Stocks, Phys. Rev. B **29**, 4217 (1984).

[19] P. B. Allen, T. P. Beaulac, F. S. Khan, W. H. Butler, F. J. Pinski, and J. C. Swihart, Phys. Rev. B **34**, 4331 (1986).

[20] H. Ebert, S. Mankovsky, D. Ködderitzsch, and P. J. Kelly, Phys. Rev. Lett. **107**, 066603 (2011).

[21] D. Ködderitzsch, K. Chadova, J. Minár, and H. Ebert, New J. Phys. **15**, 053009 (2013).

[22] J. Kudrnovský, V. Drchal, I. Turek, S. Khmelevskyi, J. K. Glasbrenner, and K. D. Belashchenko, Phys. Rev. B **86**, 144423 (2012).

[23] S. Mankovsky, D. Ködderitzsch, G. Woltersdorf, and H. Ebert, Phys. Rev. B **87**, 014430 (2013).

[24] S. Srichandan, S. Wimmer, S. Pöllath, M. Kronseder, H. Ebert, C. H. Back, and C. Strunk, Phys. Rev. B **98**, 020406(R) (2018).

[25] B. Cantor, I. T. H. Chang, P. Knight, and A. J. B. Vincent, Mater. Sci. Eng. A **375**, 213 (2004).

[26] B. Cantor, Ann. Chim. **32**, 245 (2007).

[27] Y. Zhang, G. M. Stocks, K. Jin, C. Lu, H. Bei, B. C. Sales, L. Wang, L. K. Beland, R. E. Stoller, G. D. Samolyuk, M. Caro, A. Caro, and W. J. Weber, Nat. Commun. **6**, 8736 (2015).

[28] K. Jin, B. C. Sales, G. M. Stocks, G. D. Samolyuk, M. Daene, W. J. Weber, Y. Zhang, and H. Bei, Sci. Rep. **6**, 20159 (2016).

[29] K. Jin, S. Mu, K. An, W. D. Porter, G. D. Samolyuk, G. M. Stocks, and H. Bei, Mater. Design **117**, 185 (2017).

[30] B. C. Sales, K. Jin, H. Bei, G. M. Stocks, G. D. Samolyuk, A. F. May, and M. A. McGuire, Sci. Rep. **6**, 26179 (2016).

[31] O. Gunnarsson, M. Calandra, and J. E. Han, Rev. Mod. Phys. **75**, 1085 (2003).

[32] G. V. Chester and A. Thellung, Proc. Phys. Soc. **77**, 1005 (1961).

[33] M. J. Kearney and P. N. Butcher, J Phys. C **21**, L265 (1988).

[34] S. N. F. Mott and H. Jones, *The Theory of the Properties of Metals and Alloys* (Dover, New York, 1958).

[35] R. Mahajan, M. Barkeshli, and S. A. Hartnoll, Phys. Rev. B **88**, 125107 (2013).

[36] K.-S. Kim and C. Pépin, Phys. Rev. Lett. **102**, 156404 (2009).

[37] H. Ebert, S. Mankovsky, K. Chadova, S. Polesya, J. Minár, and D. Ködderitzsch, Phys. Rev. B **91**, 165132 (2015).

[38] H. Ebert, D. Ködderitzsch, and J. Minár, Rep. Prog. Phys. **74**, 096501 (2011).

[39] H. Ebert *et al.*, Munich SPR-KKR package, version 7.7, http://olymp.cup.uni-muenchen.de/ak/ebert/SPRKKR, 2017.

[40] J. P. Perdew, K. Burke, and M. Ernzerhof, Phys. Rev. Lett. **77**, 3865 (1996).

[41] S. H. Vosko, L. Wilk, and M. Nusair, Canad. J. Phys. **58**, 1200 (1980).

[42] S. Mu, R. Olsen, B. Dutta, B. C. Larson, L. Lindsay, G. D. Samolyuk, E. D. Specht, K. Jin, H. Bei, T. Berlijn, T. Hickel, and G. M. Stocks (unpublished).

[43] See Supplemental Material at http://link.aps.org/supplemental/10.1103/PhysRevB.98.165141 for spin resolved partial density of states for $Ni_{0.5}Fe_{0.5}$, $Ni_{0.33}Co_{0.33}Fe_{0.33}$ and $Ni_{0.33}Co_{0.33}Cr_{0.33}$; convergence of zero temperature electric conductivity with the size of $k$-points mesh; and the results for exchange coupling parameters, $J_{ij}$.

[44] A. I. Liechtenstein, M. I. Katsnelson, V. P. Antropov, and V. A. Gubanov, J. Magn. Magn. Mater. **67**, 65 (1987).

[45] V. G. Vaks and N. E. Zein, Sov. Phys. JETP **40**, 537 (1975).

[46] V. G. Vaks and G. D. Samolyuk, JETP **88**, 89 (1999).

[47] R. Kikuchi, Phys. Rev. **81**, 988 (1951).

[48] J. M. Sanchez, F. Ducastelle, and D. Gratias, Physica A **128**, 334 (1984).

[49] J. L. Xu, M. van Schilfgaarde, and G. D. Samolyuk, Phys. Rev. Lett. **94**, 097201 (2005).

[50] O. K. Andersen and O. Jepsen, Phys. Rev. Lett. **53**, 2571 (1984).

[51] I. A. Abrikosov and H. L. Skriver, Phys. Rev. B **47**, 16532 (1993).

[52] I. Turek, V. Drchal, J. Kudrnovský, M. Sob, and P. Weinberger, *Electronic Structure of Disordered Alloys, Surfaces and Interfaces* (Kluwer, Boston, 1997).

[53] D. A. Broido, M. Malorny, G. Birner, N. Mingo, and D. A. Stewart, Appl. Phys. Lett. **91**, 231922 (2007).

[54] D. A. Broido, L. Lindsay, and A. Ward, Phys. Rev. B **86**, 115203 (2012).

[55] W. Li, J. Carrete, N. A. Katcho, and N. Mingo, Comput. Phys. Commun. **185**, 1747 (2014).

[56] P. Giannozzi, S. Baroni, N. Bonini, M. Calandra, R. Car, C. Cavazzoni, D. Ceresoli, G. L. Chiarotti, M. Cococcioni, I. Dabo, A. D. Corso, S. de Gironcoli, S. Fabris, G. Fratesi, R. Gebauer, U. Gerstmann, C. Gougoussis, A. Kokalj, M. Lazzeri, L. Martin-Samos, N. Marzari, F. Mauri, R. Mazzarello, S. Paolini, A. Pasquarello, L. Paulatto, C. Sbraccia, S. Scandolo, G. Sclauzero, A. P. Seitsonen, A. Smogunov, P. Umari, and R. M. Wentzcovitch, J. Phys.: Condens. Matter **21**, 395502 (2009).

[57] D. Vanderbilt, Phys. Rev. B **41**, 7892 (1990).

[58] N. E. Zein, Sov. Phys. Solid State **26**, 1825 (1984).

[59] S. Baroni, P. Giannozzi, and A. Testa, Phys. Rev. Lett. **58**, 1861 (1987).

[60] E. H. Putley, *The Hall Effect and Related Phenomena* (Butterworths, London, 1960).

[61] B. C. Sales, K. Jin, H. Bei, J. Nichols, M. F. Chisholm, A. F. May, N. P. Butch, A. D. Christianson, and M. A. McGuire, npj Quantum Mater. **2**, 33 (2017).

[62] G. D. Samolyuk, L. K. Béland, G. M. Stocks, and R. E. Stoller, J. Phys.: Condens. Matter **28**, 175501 (2016).

[63] S. Mu, G. D. Samolyuk, S. Wimmer, M. C. Troparevsky, S. Khan, S. Mankovsky, H. Ebert, and G. M. Stocks, arXiv:1806.03785.

[64] M. van Schilfgaarde and V. P. Antropov, J. Appl. Phys. **85**, 4827 (1999).

[65] G. D. Samolyuk, B. P. T. Fokwa, R. Dronskowski, and G. J. Miller, Phys. Rev. B **76**, 094404 (2007).

[66] G. Baym and L. P. Kadanoff, Phys. Rev. **124**, 287 (1961).

[67] R. E. Prange and L. E. Kadanoff, Phys. Rev. **134**, A566 (1964).

[68] T. Holstein, Ann. Phys. **29**, 410 (1964).

[69] A. V. Ruban, S. Khmelevskyi, P. Mohn, and B. Johansson, Phys. Rev. B **75**, 054402 (2007).

[70] V. Drchal, J. Kudrnovský, and I. Turek, EPJ Web Conf. **40**, 11001 (2013).

[71] P. Weiss and R. Forrer, Ann. Phys. **10**, 279 (1929).

[72] A. L. Wysocki, R. F. Sabirianov, M. van Schilfgaarde, and K. D. Belashchenko, Phys. Rev. B **80**, 224423 (2009).

[73] A. Alam and A. Mookerjee, Phys. Rev. B **72**, 214207 (2005).

[74] *Thermal Conductivity: Theory, Properties, and Applications*, edited by T. M. Tritt (Kluwer, New York, 2004).

[75] C. Y. Ho, M. W. Ackerman, K. Y. Wu, T. N. Havill, R. H. Bogaard, R. A. Matula, S. G. Oh, and H. M. James, J. Phys. Chem. Ref. Data **12**, 183 (1983).